Publications of the Astronomical Society of the Pacific, **118**: 1574–1590, 2006 November

Performance Modeling of a Wide-Field Ground-Layer Adaptive Optics System

David R. Andersen,[1] Jeff Stoesz,[1] Simon Morris,[2] Michael Lloyd-Hart,[3] David Crampton,[1] Tim Butterley,[2] Brent Ellerbroek,[4] Laurent Jolissaint,[1] N. Mark Milton,[3] Richard Myers,[2] Kei Szeto,[1] Andrei Tokovinin,[5] Jean-Pierre Véran,[1] and Richard Wilson[2]

Received 2006 April 20; accepted 2006 September 14; published 2006 November 29

ABSTRACT. Using five independent analytic and Monte Carlo simulation codes, we have studied the performance of wide-field ground-layer adaptive optics (GLAO), which can use a single, relatively low order deformable mirror to correct the wave-front errors from the lowest altitude turbulence. GLAO concentrates more light from a point source in a smaller area on the science detector, but unlike with traditional adaptive optics, images do not become diffraction-limited. Rather, the GLAO point-spread function (PSF) has the same functional form as a seeing-limited PSF and can be characterized by familiar performance metrics such as full width at half-maximum (FWHM). The FWHM of a GLAO PSF is reduced by 0.″1 or more for optical and near-infrared wavelengths over different atmospheric conditions. For the Cerro Pachón atmospheric model, this correction is even greater when the image quality is poorest, which effectively eliminates "bad seeing" nights; the best seeing-limited image quality, available only 20% of the time, can be achieved 60%–80% of the time with GLAO. This concentration of energy in the PSF will reduce required exposure times and improve the efficiency of an observatory up to 30%–40%. These performance gains are relatively insensitive to a number of trade-offs, including the exact field of view of a wide-field GLAO system, the conjugate altitude and actuator density of the deformable mirror, and the number and configuration of the guide stars.

1. INTRODUCTION

The idea that the turbulence of the atmosphere can be corrected by adaptive optics (AO) is not new (Babcock 1953), but there have always been limitations to the approach. One of the more serious is that classical or single guide star AO systems produce only a small corrected field of view (FOV); isoplanatic errors cause the image quality to quickly degrade from the center of the corrected field. Typically, the spatial resolution falls below the diffraction limit in the near-infrared only 30″ from the guide star. This small and nonuniform corrected FOV severely limits the sky coverage of traditional AO systems, and even limits sky coverage for those that employ laser guide stars (LGSs; first proposed by Foy & Labeyrie 1985). Another limitation of traditional AO systems is that the performance decreases from the near-infrared to the visible; to fully correct the turbulence in the optical would require deformable mirrors (DMs) with many more actuators and a control system operating at a much higher frequency (Dekany et al. 2006). Finally, existing AO systems perform well only when the image quality conditions are good; if the seeing is poor, control bandwidths and DM actuator strokes and densities are insufficient to maintain diffraction-limited imaging.

In the near future, multiconjugate adaptive optics (MCAO) systems (Johnston & Welsh 1991; Ragazzoni 1999; Beckers 2000; Ragazzoni et al. 2000; Flicker et al. 2000) promise to produce a larger corrected FOV with improved sky coverage, by employing multiple DMs and wave-front sensors (WFSs), but will still be limited to observations in the near-infrared on nights with average or better image quality. While the availability of MCAO systems will change the use of observatories, it is important to realize that today a large fraction of ground-based astronomical research still relies on seeing-limited observations at optical wavelengths. Ground-layer adaptive optics (GLAO) was proposed to circumvent these limitations of traditional AO systems by applying a limited AO correction to an even larger FOV under any atmospheric conditions, even at optical wavelengths (Rigaut 2002). A GLAO system does not attempt to produce diffraction-limited images; instead, it attempts to improve the concentration of the point-spread function (PSF) by sensing and correcting only the lowest turbulent layers of the atmospheres. Because the corrected layers are so close to the ground, the correction is the same over the entire large FOV. Uncorrected turbulent layers at higher altitudes degrade the spatial resolution isoplanatically. The use of GLAO

[1] Herzberg Institute of Astrophysics, National Research Council of Canada, 5071 West Saanich Road, Victoria, BC V9E 2E7, Canada; david.andersen@cnrc-nrc.gc.ca.

[2] Department of Physics, University of Durham, Rochester Building, Science Laboratories, South Road, Durham DH1 3LE, UK.

[3] Steward Observatory, University of Arizona, 933 North Cherry Avenue, Tucson, AZ 85721.

[4] Thirty Meter Telescope Project, 1200 East California Boulevard, Mail Code 102-8, Pasadena, California 91125.

[5] Cerro Tololo Inter-American Observatory, Casilla 603, La Serena, Chile.

TABLE 1
INTEGRATED TURBULENCE $J = \int C_n^2\, dh$ FOR "GOOD," "TYPICAL," AND "BAD" GROUND AND FREE ATMOSPHERES

Altitude (m) (1)	Good J (10^{-14} m$^{1/3}$) (2)	Typical J (10^{-14} m$^{1/3}$) (3)	Bad J (10^{-14} m$^{1/3}$) (4)
0	9.26	7.04	13.8
25	1.83	2.25	10.8
50	0.574	1.35	15.3
100	0.362	1.24	15.8
200	0.614	1.99	10.3
400	0.960	2.87	6.46
800	1.18	3.02	7.29
1600	0.913	1.75	6.77
3600	...	...	32.0
5500	...	17.0	...
8400	9.00	...	...

NOTE.—Altitudes >3 km are considered "free."

can therefore complement MCAO surveys; the survey efficiency of a GLAO system, as we show, continues to increase as the FOV increases and actually surpasses that of a MCAO system. MCAO or classical AO can then be used for follow-up observations of individual discoveries made from GLAO surveys.

Early simulations suggested that GLAO could produce images with a full width at half-maximum (FWHM) less than 0.″2 in the J band. Caution should be used when evaluating early GLAO modeling results, however, because they are critically dependent on the input turbulence profiles. As Tokovinin (2004) pointed out, studies of GLAO require accurate knowledge of the atmosphere below ~2 km, in addition to knowing the turbulence profile of the free atmosphere. Specifically, turbulent layers at intermediate altitudes, which Tokovinin called the gray zone, will only be partially corrected and will also introduce residual anisoplanatism. Earlier work on GLAO focused on FOVs less than 3′ (Baranec et al. 2003; Tokovinin 2004; LeLouarn & Hubin 2004; Hubin et al. 2004; Jolissaint et al. 2004; Stoesz et al. 2004).

Here we examine the performance of a GLAO system over FOVs greater than 5′ in size, using new, higher resolution turbulence profiles. This work was carried out in order to study the potential of a GLAO system at the Gemini Observatory, but the results are applicable to 10 m class telescopes in general. The results presented here are based on a set of model atmospheres that were derived at least in part from balloon measurements of the turbulence over Cerro Pachón, Chile, that had a vertical resolution of 6 m (Tokovinin & Travouillon 2006). After describing these model atmospheres in § 2, we present the analytic and Monte Carlo modeling tools used for this study in § 3. We also reconcile the results of these codes, which lends greater confidence to the results. Section 4 describes the GLAO PSF and relevant performance metrics. We apply these metrics in analyzing a baseline wide-field GLAO system in § 5 and describe various trade-offs on this baseline in § 6. Finally, § 7 provides a summary of our modeling results and a discussion of the promising future of GLAO.

2. MODEL ATMOSPHERES

GLAO system performance depends crucially on the structure of the atmospheric turbulence profile. In particular, the size of the compensated field and the uniformity of the delivered PSF over the field depend on the thickness of the boundary layer, while the overall degree of image improvement depends sensitively on the ratio of aberrations in the boundary layer to those in the free atmosphere. Historically, these are not quantities that have been studied in detail because, prior to the emergence of GLAO as a potentially valuable observing tool, they were not seen as important measures of a site's quality.

Fortunately for our study, detailed measurements of the structure of atmospheric turbulence with a resolution of 6 m in the boundary layer (altitudes below 5000 m) recorded from 43 balloon flights exist as part of the 1998 Gemini South (Gemini-S) seeing campaign at Cerro Pachón (Vernin et al. 2000). The atmospheric turbulence profiles used in this study have been derived from those balloon data and also from MASS/DIMM (multiaperture scintillation sensor/differential image motion monitor) data taken from Cerro Pachón in 2003 (Tokovinin & Travouillon 2006; see also Tokovinin et al. 2003). While more site testing is required to confirm the presence of strong ground-layer turbulence at other sites, the results of GLAO simulations using the high-resolution atmospheric data from Cerro Pachón should be generally applicable to other telescope sites.

In order to reduce the magnitude of the modeling task, a total of nine atmospheric profiles have been constructed from the balloon flight data, representing a broad range of typical conditions. Three turbulence profiles for the atmosphere below 2 km in altitude were computed, representing the averages of the best 25%, worst 25%, and central 50% of the data, sorted by r_0. Similarly, the free atmosphere above 2 km was represented by a single layer of turbulence, with C_n^2 and height determined again from the best (25%), worst (25%), and typical (50%) conditions for the upper atmosphere. Essentially, no degree of correlation between the strengths of the boundary layer and the free atmosphere was found (Tokovinin 2003), so nine profiles were constructed by matching the three boundary-layer profiles with each of the three upper atmosphere layers. Table 1 gives the altitudes and integrated turbulence values ($J = \int C_n^2\, dh$ in m$^{1/3}$) for each of these profiles. Column (1) of this table is the effective height of each layer above the site level, as defined by the integral $\int hC_n^2\, dh/J$, and the remaining columns are the integrated turbulence values for each model profile. The lowest layer was assigned a height of zero in this study. The approximate probabilities of occurrence, given the percentiles that the profiles were drawn from, are given in Table 2. Figure 1 shows good agreement between the cumulative probability distribution from the model predictions to measurements made from Gemini-S. Hence, the results

TABLE 2
PROBABILITIES USED TO WEIGHT ATMOSPHERIC MODELS

	Ground-Layer Atmosphere		
Free Atmosphere	Good	Typical	Bad
Good	0.0625	0.125	0.0625
Typical	0.125	0.250	0.125
Bad	0.0625	0.125	0.0625

of our simulations should be representative of the conditions at Cerro Pachón during the four 1 week balloon missions that took place in all four seasons of 1998. We refer to these nine atmospheric models as two-word (or two-letter) designations for the ground- and free-atmosphere profiles, respectively. For example, good : typical (G:T) refers to the model atmosphere consisting of the "good" (i.e., largest r_0) ground-layer profile and the "typical" (median r_0) free-atmosphere profile. A caveat of the results presented here is that while the profiles exhibit a wide range of r_0 values, almost all have similar isoplanatic angles, θ_0; in all cases, we assumed an outer scale of $L_0 = 30$ m (Table 3).

3. MODELING TOOLS

In assessing the expected performance of GLAO, five simulation codes written by four groups have been used. These were thoroughly tested and compared to one another to ensure a high degree of confidence in the results. Three codes implement analytic calculations, while the remaining two codes are full-wave propagation Monte Carlo simulations. Analytic codes, which calculate an estimate of the long-exposure AO-corrected PSF using the fact that the optical transfer function is proportional to the negative exponential of the aperture-averaged structure function of the residual phase disturbances in the telescope pupil, were generally used to explore large parameter spaces and study various performance trade-offs. Monte Carlo models are much more computationally intensive and were used primarily to study physical effects not incorporated into analytic models and to verify the analytic model results for the baseline configurations.

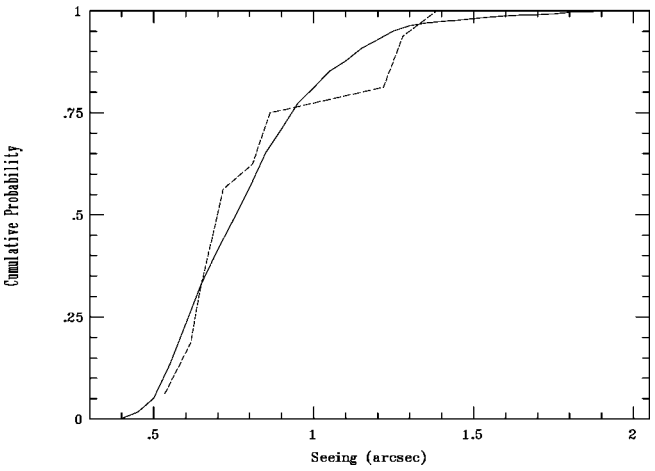

FIG. 1.—Cumulative histogram of Gemini-S seeing measurements in the *R* band, with probabilities of the model atmospheric profiles overplotted (*dashed line*). The measurements were made from Gemini-S acquisition camera data corrected to zenith (data available at http://www.gemini.edu/metrics/seeing.html). There is good agreement between these curves; the probabilities of the derived atmospheric profiles are within present experimental uncertainty.

3.1. PAOLA Analytic Modeling Tool

One of the analytic modeling codes, PAOLA (Performance of Adaptive Optics for Large Apertures; Jolissaint & Véran 2002; Jolissaint et al. 2006), was developed at NRC-HIA (National Research Council of Canada's Herzberg Institute of Astrophysics) and is now used by more than a dozen groups throughout the world. It models the effect of the AO correction as a spatial-frequency filtering of the turbulent phase power spectrum, from which the AO long-exposure PSF in any direction is easily derived. One can identify five basic limitations on any classical AO system, and these are taken into account in the PAOLA code:

1. *Anisoplanatism*.—In GLAO mode, the DM commands are assumed to be derived from an average of the multiple guide star WFS measurements. The difference between this average command and the actual turbulent phase at a given point in the field is called the anisoplanatic error and is de-

TABLE 3
VALUES OF r_0 AND θ_0, AND SEEING FOR ALL NINE C_n^2 PROFILES USED IN THIS STUDY

	Ground-Layer Atmosphere (Good)			Ground-Layer Atmosphere (Typical)			Ground-Layer Atmosphere (Bad)		
Free Atmosphere	r_0 (m)	θ_0 (arcsec)	FWHM (arcsec)	r_0 (m)	θ_0 (arcsec)	FWHM (arcsec)	r_0 (m)	θ_0 (arcsec)	FWHM (arcsec)
Good	0.189	2.61	0.535	0.164	2.59	0.616	0.083	2.52	1.218
Typical	0.157	2.72	0.644	0.141	2.70	0.717	0.079	2.62	1.279
Bad	0.125	2.84	0.809	0.117	2.82	0.864	0.073	2.73	1.385

NOTE.—Seeing was in arcseconds at 500 nm.

scribed in Stoesz et al. (2004) for the case of multiple natural guide star GLAO. It is important to note that this error term is by far the most important for GLAO.

2. *Fitting error*.—The number of WFS lenslets (and/or DM actuators) defines the number of aberration modes that can be corrected by the system and, in particular, sets the highest spatial frequency that can be measured and corrected. Uncorrected high-spatial-frequency aberrations are transmitted to the output of the AO system, giving rise to what is called the fitting error, due to the limited ability of the system to adjust (fit) itself to the incident phase. Fitting error is the next most important source of residual aberrations for GLAO.

3. *WFS spatial aliasing*.—These same uncorrected high-frequency aberrations are seen by the WFS as low-spatial-frequency errors and are aliased in the low-frequency domain of the WFS. Aliasing error is the third important GLAO error source.

4. *WFS noise*.—This error is due to the guide star photon noise, WFS detector read noise, and WFS dark current noise.

5. *System servo lag*.—To achieve a sufficient signal-to-noise ratio (S/N) on the phase measurement, the WFS has to integrate over a given exposure time. Determining the exposure time involves a trade-off between getting enough guide star photons and averaging out the high-temporal-phase fluctuations. Moreover, the reading of the WFS, the phase reconstruction, and the DM surface update takes some time (roughly one sampling period), creating a time lag between phase measurement and correction. The phase-error term associated with both time averaging and time lag is called the servo-lag error.

The AO loop controller is modeled in PAOLA as a simple integrator. Such an analytical approach is very computationally efficient and permits PAOLA to model AO performance across large parameter spaces in a reasonable period of time. However, it can only account for the fundamental limits of the AO correction, so the performance estimates need to be refined with much more computationally intensive Monte Carlo simulation tools (see §§ 3.4 and 3.5), taking into account nonlinear and/or second-order effects (correlated effects, sensitivity to vibrations, cone effect, spot elongation, etc.) once a reduced set of suitable parameters has been found.

3.2. CIBOLA

CIBOLA (Covariance—Including Basic Option for Linear Analysis; Ellerbroek 2005) is a second analytical modeling tool that combines and extends features of PAOLA and prior analytical models for tomographic wave-front reconstruction and MCAO (Tokovinin & Viard 2001; Tokovinin 2002). This code can be used to assess the correlated effect of five fundamental error sources (DM fitting error, WFS spatial aliasing, WFS measurement noise, finite servo bandwidth, and anisoplanatism) for AO systems, incorporating one or more DMs and WFSs. Narrow and wide-field performance estimates can be obtained in terms of wave-front error power spectra and PSFs, computed using conventional, MCAO, or GLAO control algorithms.

The principal capabilities and limitations of CIBOLA are derived from the use of spatial filtering approximations for all of the basic wave-front propagation, sensing, reconstruction, and correction operators encountered in classical linear systems modeling of adaptive optics. This approach enables rapid analysis of AO systems, which is sufficiently accurate for many applications, but also neglects aperture edge effects and is (rigorously) limited to the case of natural guide stars.

3.3. Arizona Analytic Code

The IDL-based analytic GLAO simulation tool used at the University of Arizona was originally developed by Tokovinin (2004). A multilayer residual structure function for each beacon is computed from the von Kármán power spectrum at each turbulent layer, accounting for the geometry of the beacon constellation. The model assumes that a single natural guide star is used for sensing global tilt. The effects of temporal delay and WFS noise are neglected.

3.4. Arizona Monte Carlo Simulation Code

The Monte Carlo simulation tool written at the University of Arizona, described by Lloyd-Hart & Milton (2003), supports an arbitrary number of LGSs, natural guide stars (NGSs), DMs, and atmospheric turbulence layers. The model assumes the geometric optics approximation. Atmospheric turbulence and DM corrections are represented as vectors of coefficients of the Zernike modes. An analytic computation is used to obtain the influence of atmospheric turbulence at each layer within the intersecting cone for each LGS and NGS. The net aberration for an object at infinity is also computed analytically.

The reconstruction matrix is built from the product of the maximum a priori (MAP) inverse of the DM influence matrix and the atmospheric-layer influence matrix. Random-turbulence Zernike coefficient vectors are generated from the Cerro Pachón atmospheric models using Kolmogorov statistics for the Zernike polynomials of order $1 \leq n \leq 30$ (i.e., the first 496 Zernike polynomials). DM corrections are the product of these random-turbulence Zernike coefficient vectors and the reconstruction matrix. Read noise with Gaussian statistics and Poisson photon noise are simulated for a Hartmann-Shack WFS and added to the noise-free wave-front corrections.

The performance of each candidate GLAO beacon configuration is evaluated by calculating the rms wave-front deviation at a range of different field positions out to the full field radius. The expected uncorrected rms error for Zernike modes of order $n > 30$ is added to account for high-frequency modes not included in the simulation.

TABLE 4
PARAMETERS OF THE COMMON MODELS USED TO VALIDATE THE SIMULATION CODES

Parameter	Value
Atmosphere	$r_0 = 17$ cm at $\lambda = 500$ nm; $L_0 = 30$ m
	C_n^2 profiles (fractional power at each height):
	Height (m) 0 300 500 900 2000 10,000
	Profile 1: 0.45 0.15 0.00 0.00 0.07 0.33
	Profile 2: 0.30 0.00 0.30 0.00 0.07 0.33
	Profile 3: 0.20 0.00 0.00 0.40 0.07 0.33
Telescope	Outer diameter = 8.0 m; no central obscuration
FOV	$10' \times 10'$
Guide stars	Five NGSs on a regular pentagon in a circle of radius 7.′07
	Brightness:
	Case 1: infinite
	Case 2: $R = 13$ (85,400 photons m^{-2} s)
WFS	10×10 Shack-Hartmann, 8×8 pixels per subaperture
	Plate scale: 0.″2 $pixel^{-1}$
	Read noise: 3.5 e^- rms per readout $pixel^{-1}$
	Frame rate: 500 s^{-1}
	Wavelength: 700 nm monochromatic
	No sky background
DM	Conjugate height: 0 m
	Compensation: $\leq$77 dof
Test stars	Coordinates: (0.′0, 0.′0), (2.′5, 0.′0), (5.′0, 0.′0), (2.′5, 2.′5), (5.′0, 5.′0)
	Wavelength: 1.25 μm monochromatic
	Plate scale: 0.″1 $pixel^{-1}$
	Integration time: $\geq$100 s

3.5. Durham Monte Carlo AO Model

The University of Durham (UD) Monte Carlo AO model includes detailed WFS noise propagation, produces two-dimensional PSFs, and was used to quantify the effects of such noise on PSF parameters across the GLAO field for various seeing and noise conditions and zenith angles. The capabilities of the UD Monte Carlo code are summarized as follows:

1. The atmospheric model can cope with a large (not specifically limited) number of independently moving turbulent layers.
2. Multiple laser beacons and/or NGSs can be modeled.
3. Multiple DMs of a number of types can be modeled.
4. Multiple WFSs (one per laser beacon or NGS) can be included. These include all main detector noise effects, as well as the effects of detector pixellation and atmospherically induced speckle.
5. The science PSF may be sampled at a number of field points.

3.6. Direct Comparison of Results

Starting with the same inputs (Table 4), three figures of merit were computed for PSFs compensated with GLAO: FWHM, ensquared energy within 0.″1, and Strehl ratio. Three turbulence profiles were run both with and without photon and read noise included. In all models, spatial fitting error was included, and some included WFS aliasing error. Other sources of residual wave-front error, such as servo lag, were omitted. The intention was not to produce realistic estimates of performance at Gemini-S , but rather to verify that the codes all predicted essentially the same results (this was not true initially, but excellent agreement was eventually achieved).

The results from the five codes are summarized in Figure 2 and demonstrate agreement to within ~0.″02 in the PSF FWHM. The two Monte Carlo codes generally predict somewhat worse performance than the three analytic codes, presumably because of the inclusion in the Monte Carlo simulations of a greater range of physical effects.

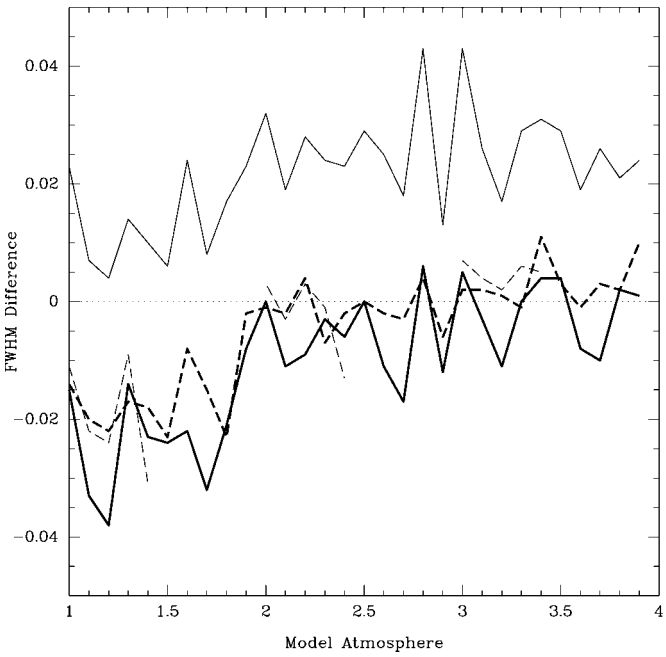

FIG. 2.—Difference in simulated FWHM between various simulation codes and the UD Monte Carlo model for various model atmospheres, field positions, and treatments of noise presented in Table 4. The Arizona Monte Carlo code results are marked with a thin solid line (the residuals are all greater than 0), the Arizona analytic code results are marked with a thin dashed line, the PAOLA results are marked with a thick dashed line, and the CIBOLA results are marked with a thick solid line. Results between 1 and 1.9 use profile 1 from Table 4, results between 2 and 2.9 use profile 2, and results between 3 and 3.9 use profile 3. The 10 PSF residuals shown for each profile are made from five field positions with and without the inclusion of noise. Results labeled with numbers greater than or equal to one-half for each profile came from simulations including noise. For an absolute sense of scale, the UD model FWHM for 1.0 is 0.″235, 2.0 is 0.″258, and 3.0 is 0.″307. Regardless of the details of the fits, model atmospheres, or inclusion of noise, the five GLAO simulation codes produced FWHMs that agreed to within 0.″04. In most cases, the agreement was even better. The analytic codes produced virtually indistinguishable results; the Monte Carlo codes, which included a greater range of physical effects, produced corrected FWHMs that were not quite as narrow in most cases.

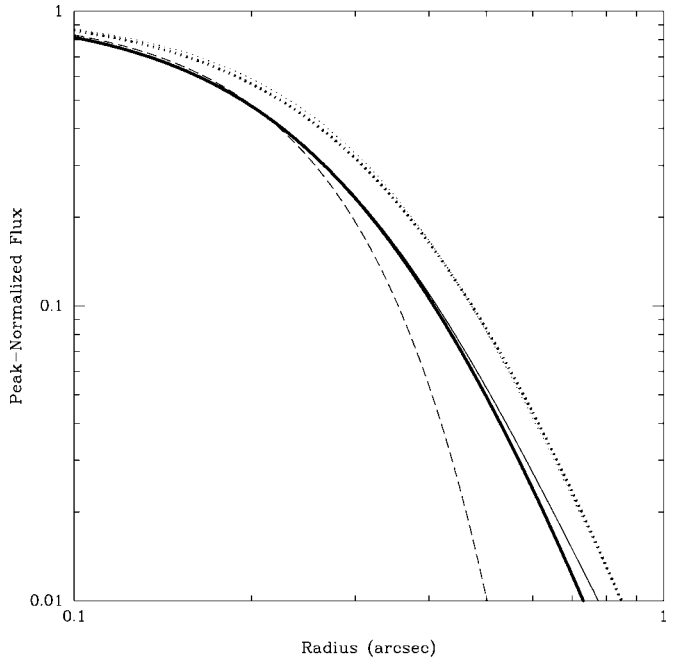

FIG. 3.—Radial profile of GLAO-corrected PSFs in normalized flux vs. radius (*thick solid line*). The seeing-limited PSF is marked with a thick dotted line (to the right of the thick solid line). Gaussian (*dashed line*) and Moffat (*thin solid line* to GLAO PSF; *thin dotted line* to seeing-limited PSF) fits are marked as well. A Moffat function with $\beta = 2.9$ provides an excellent fit to both the GLAO and seeing-limited PSFs in this case. The PSF was generated at a wavelength of 1.0 μm.

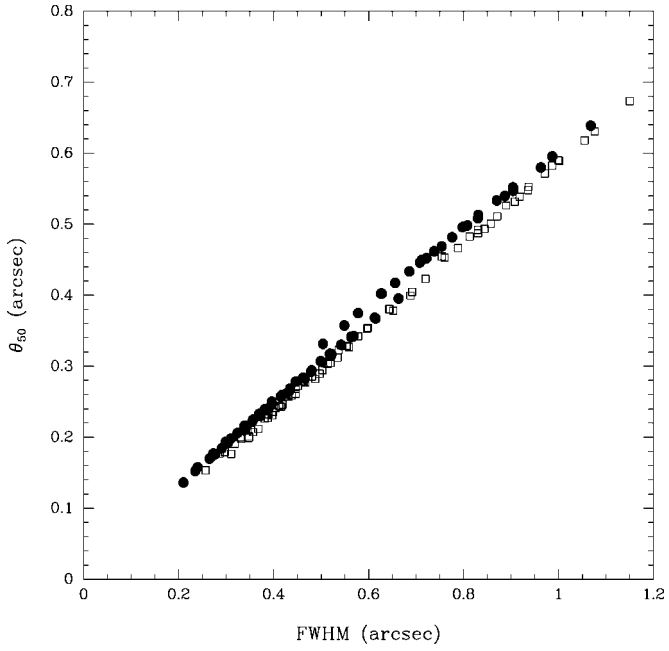

FIG. 4.—FWHM vs. radius enclosing 50% of the total energy for a variety of wavelengths and turbulence profiles. The squares are results for seeing-limited PSFs, and the circles show results of GLAO-improved PSFs. The two parameters are strongly correlated, which indicates that the shape (i.e., the Moffat β parameter) of the PSF does not change significantly in these simulations. There are two sequences apparent in the GLAO PSFs. The points in the upper sequence were simulated using the "bad" ground-layer turbulence profile. In this case, it appears that the core of the PSF is improved with GLAO, but that the PSF halo is slightly stronger, which leads to a comparatively larger half-light radius. The overall tight relation between half-light radius and FWHM means that both parameters are valuable GLAO merit functions.

4. TOOLS FOR EVALUATING GLAO PERFORMANCE

The PSF from a GLAO system is very different from the PSF of a diffraction-limited AO system. Therefore, the proper merit functions for evaluating a GLAO system need to be identified. We begin this process by describing the functional form of the GLAO PSF and then present and discuss various performance metrics we use to gauge the performance of GLAO.

4.1. The GLAO PSF

The PSF produced by a wide-field GLAO system exhibits no diffraction-limited peak and qualitatively is very similar to the PSF generated without any form of AO. The shape of the GLAO PSF shown in Figure 3 is well fit by the same function commonly used to describe seeing-limited PSFs, the Moffat function (Moffat 1969):

$$I(r) = I_0\left[1 + \left(\frac{r}{\alpha}\right)^2\right]^{-\beta}. \quad (1)$$

A Gaussian profile matches the profile shape only to roughly 50% of the peak flux, while the Moffat function provides a good fit below 1% of the peak height. Based on our simulated PSFs, both the GLAO PSF and seeing-limited PSF are well fit by a Moffat PSF with β between 2.5 and 4.5.

4.2. GLAO Merit Functions

As part of the Gemini feasibility study, a reasonably detailed science case was prepared for GLAO. Science requirements for GLAO with representative instruments were then defined. Proper modeling of the science gains from a GLAO system requires the full PSF information. However, for many of the science cases, a few key parameters that gave a reasonable (but simplified) understanding of the gains were identified. We present and discuss several of these merit functions here:

1. *Full width at half-maximum*.—A familiar and easily calculable quantity is the FWHM of the PSF. For proper motion studies or work on crowded stellar fields, at least with the expected GLAO PSF shapes, FWHM is a key parameter.

2. *Half-light radius (θ_{50})*.—The radius enclosing 50% of the total energy—the half-light radius—is a particularly valuable merit function if the shape of the PSF is not well understood. A correlation exists between θ_{50} and FWHM (Fig. 4), but be-

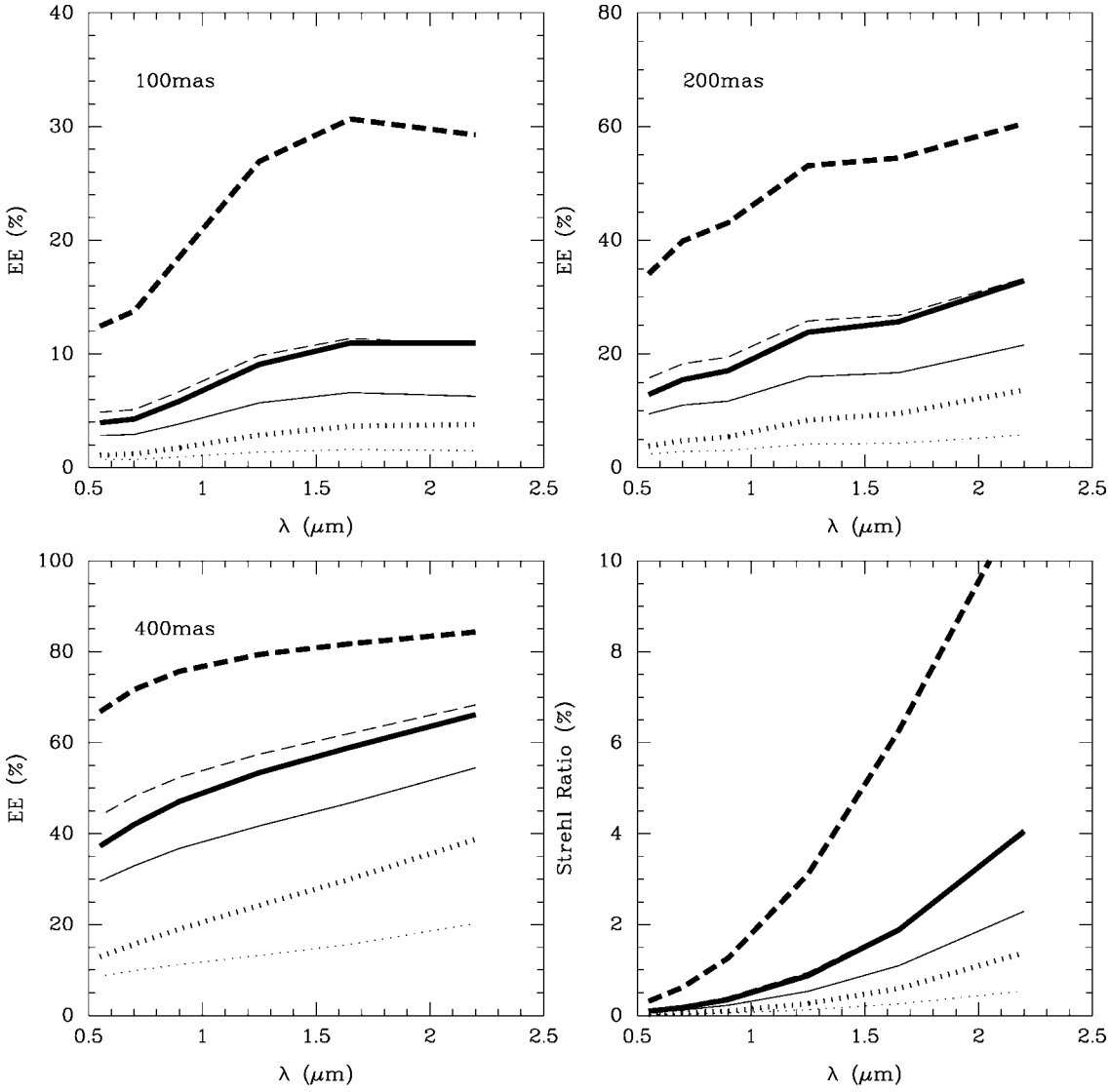

FIG. 5.—EE within 100, 200, and 400 mas, and Strehl ratio vs. wavelength for bad : bad (*dotted lines*), typical : typical (*solid lines*), and good : good (*dashed lines*). Thick lines show the GLAO performance, while thin lines show the seeing-limited measurements. The EE within 100 mas is less than 10% at most wavelengths and for most turbulence profiles. Only 20% of the EE is within 200 mas in most cases. The Strehl ratio is very low for wide-field GLAO observations and is less than 4% in most cases (except for the good : good performance at $\lambda > 1.5$ μm).

cause of the variation in the Moffat parameter β, the half-light radius may be a better general merit function, since it is more tightly correlated with the integration time ratio discussed below.

3. *Ensquared energy (EE).*—Measured within an aperture (we used 0.″1 and 0.″2 apertures), EE is an important merit function for spectroscopy, as it indicates the amount of energy that enters a slit of a given size. The EE within 100 or 200 mas is small at most scientific wavelengths, however, as shown by Figure 5.

4. *Integration time ratio (ITR).*—Defined as the ratio of required exposure times to reach a given S/N in the optimal aperture in the background-limited case without and with GLAO; the higher the value of ITR, the greater the GLAO performance gain. ITR is especially relevant to science cases requiring faint, pointlike object imaging. As expected from the S/N equation, ITR is proportional to the square of the ratio of seeing-limited to GLAO θ_{50} (Fig. 6).

5. *Image quality variation.*—An important scientific criterion to consider is the image quality variation over the scientific FOV. In practical terms, PSF uniformity across the FOV will make observations easier to calibrate, reduce, and interpret. As we discuss below, however, image quality variation is critically dependent on the FOV being averaged (Fig. 7). If areas near guide stars are included in the measure of image quality var-

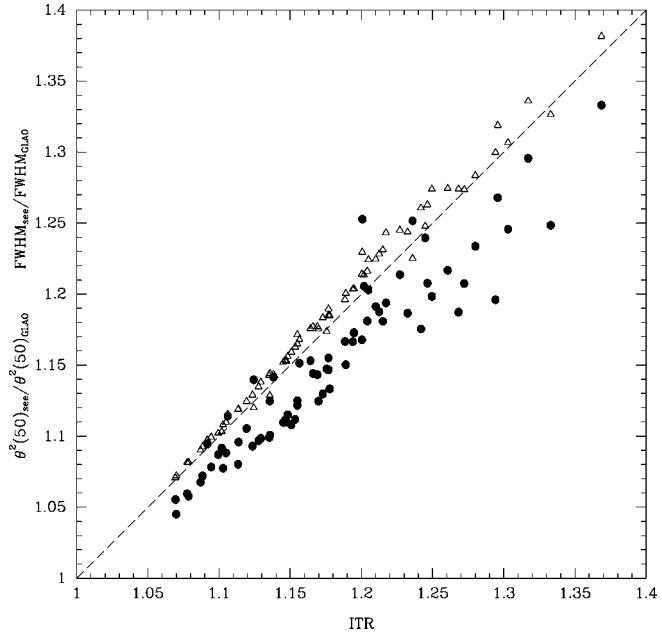

FIG. 6.—ITR vs. the ratio of seeing-limited to GLAO-corrected FWHM (*circles*), and the square of the ratio of seeing-limited to GLAO-corrected half-light radius θ_{50} (*triangles*) for a range of wavelengths and turbulence profiles. While both FWHM and $(\theta_{50})^2$ ratios are good proxies for ITR, it should be noted that the correlation between ITR and the $(\theta_{50})^2$ ratio is significantly tighter.

iation, that variation will increase substantially. In general, image quality is very uniform over interesting FOVs.

6. *Strehl ratio*.—An important merit function for classical AO systems, the Strehl ratio is defined as the ratio of the PSF peak flux to the peak flux of the perfectly diffraction-limited PSF. However, Strehl ratio has little meaning for a GLAO system; at a wavelength of 1.25 μm, all codes predict less than 2% Strehl ratios (Fig. 5).

For making general comparisons between the GLAO performance and seeing-limited performance, the FWHM and θ_{50} are the most useful parameters. EE is the most interesting merit function for a specific spectrograph slit size, but the gains measured from EEs are very sensitive to the size of the slit aperture; very small absolute GLAO performance gains will be found if the aperture is significantly smaller than the FWHM, because very little light will make it through a narrow slit aperture in either the GLAO or seeing-limited case. The largest absolute and relative GLAO performance gain is found if the aperture size approaches the GLAO FWHM (Fig. 5), which follows, since the radial profile of the GLAO PSF is falling at the given aperture slit width while the radial profile of the seeing-limited PSF is still relatively flat and near the peak value. We therefore adopt the FWHM as the primary GLAO performance metric throughout the course of this work and cite EE or ITR only when relevant.

5. PERFORMANCE OF A WIDE-FIELD GLAO SYSTEM

Based on initial results of simulations that showed that the performance of GLAO systems is relatively insensitive to the specific LGS asterism and FOV (see § 6), a baseline GLAO configuration was adopted, which employs four sodium LGSs arranged in a square, with each beacon 5′ from the center. When used, we adopt an asterism of three equally bright NGSs arranged in a triangle (Fig. 8; NGSs used for correcting tip-tilt are only used in the Monte Carlo simulations). We used WFSs with a relatively small number of subapertures; only 10–17 samples across the diameter of the DMs or WFSs were used (between 77 and 227 total subapertures), depending on the simulation, because a high-order correction is not necessary to achieve a good GLAO correction (see § 6.2.1). We averaged the signal from the four LGS WFSs so that the uncorrelated signal would cancel on average, leaving only the common signal from the ground layer. The deviations in wave fronts caused by layers over 2 km will be uncorrelated. We modeled a GLAO system that employed an adaptive secondary mirror (first proposed by Beckers 1989) conjugated to −97 m, capable of correcting between 80 and 230 modes, depending on the WFS architecture (−97 m is the conjugate altitude of the current nonadaptive secondary mirrors of the Gemini telescopes; as § 6.2.2 shows, the results of simulations are relatively insensitive to the conjugate altitude). The performance of the GLAO system was modeled at four scientific wavelengths: 0.7, 1, 1.65, and 2.2 μm, corresponding roughly to the *R*, *J*, *H*, and *K* bands, respectively.

5.1. Image Quality Improvement

At all wavelengths studied and for most model atmospheres, we find that GLAO will decrease the FWHM of a PSF by roughly 0.″1. However, the fractional change in PSF FWHM varies significantly from a factor of 3.8 improvement in the *K* band with the bad : good profile, to just a factor of 1.1 improvement in the *R* band with the typical : bad profile. The performance improvement is greatest when the ground-layer turbulence is large (Fig. 9). This means that the best image quality conditions that occur, without GLAO, only 20% of the time, occur 60%–80% of the time with a GLAO system, transforming the cumulative distribution of image quality (Fig. 10). In particular, poor image quality conditions occur only rarely once a GLAO system is employed.

The expectation from previous studies (Rigaut 2002) was that the *J*-band GLAO FWHM should be roughly 0.″2. As Figures 9 and 10 show, the results presented here are more pessimistic. Simulations of the PSF using only the free-atmosphere turbulence showed that even for a perfect GLAO correction the FWHM is greater than 0.″2 under most atmospheric conditions. We note that the full GLAO simulation of atmospheres with "bad" free atmospheres yields a smaller FWHM than from simulations of seeing-limited observations

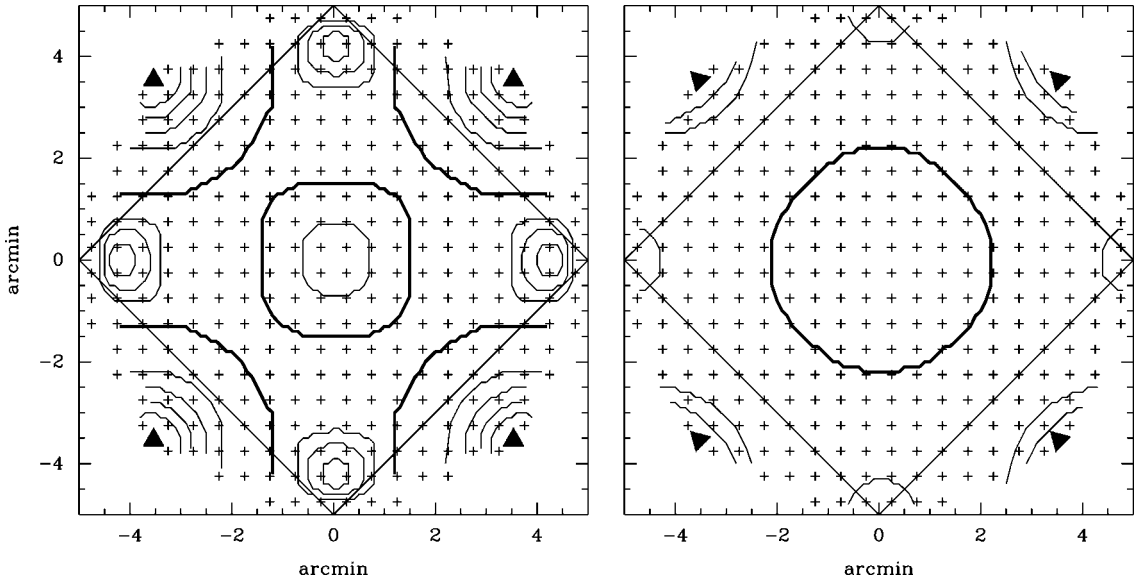

FIG. 7.—EE in 0.″2 (*left*) and FWHM (*right*) contours of the GLAO PSF for the good : good turbulence profile as measured at 2.2 μm. A $7' \times 7'$ FOV is marked, as are each of the points simulated using PAOLA (plus signs). LGS locations are marked with filled triangles. The performance is very uniform across the FOV; the separations between contours is just 1% in EE and 0.″01 in FWHM. The thick lines correspond to contours of lowest EE in 0.″2 (49%) and largest FWHM (0.″19). Near a LGS, the wave-front error will be reduced because the average of the pupils will be more heavily weighted by the turbulence from the free atmosphere in the direction of the LGS, thus leading to an improvement in image quality. Then, as one moves away from the direction of a LGS beacon, the performance will drop due to anisoplanatism. However, in the direction between two LGSs, the total wave-front error will again decrease (and image quality will improve) because now the wave-front error due to free-atmosphere turbulence in that direction will be measured by two LGS WFSs and will not cancel. In the center of the FOV, the image quality will again improve very slightly, as all four LGS WFSs will sense a fraction of the turbulence from higher layers. In essence, the "gray zone" is field-dependent and is slightly higher in the field center, so more turbulence is corrected. If the scientific FOV can be chosen such that the LGSs are out of it, the correction across the FOV will be very uniform, which makes data reduction and calibration easier.

that included only the free atmosphere. This is due to the relatively low altitude of the "bad" free atmosphere (3 km), which is being partially corrected by the GLAO simulations. Measured FWHMs greater than 0.″4 were initially attributed to a number of different factors, but as we show in § 6, the results are relatively insensitive to various trade-offs. We believe that the superior GLAO performance quoted above can be primarily attributed to the adoption of simpler, more optimistic model atmospheres. The larger number of ground layers for our model atmospheres, combined with the probabilities of given atmospheric conditions occurring, produce more realistic estimates of GLAO performance gains (which are still significantly improved over the seeing-limited performance).

Despite these lower estimates of GLAO-corrected FWHMs provided by our models, the gains in observing efficiency are still dramatic. Assuming background-limited imaging and an optimal point-source extraction radius, one can combine the GLAO gains using the model atmosphere probabilities listed in Table 2 to estimate GLAO efficiency gains between 1.5 and 2.0 at different scientific wavelengths (Fig. 11). This can translate into a substantial gain for an observatory; based on the Gemini Observatory 2004B proposal statistics, GLAO would benefit 55% of the programs (proposals requesting observations between 0.6 and 2.2 μm that do not require high-order AO) and would improve the efficiency of the whole observatory by a factor of up to 30%–40%.

5.2. Performance Off-Zenith

The performance off-zenith was studied assuming bright NGSs with the typical : typical atmospheric profiles. Field quadrant averages and standard deviations for all parameters measured at a wavelength of 1.6 μm are given in Table 5. As expected, the performance decreases off-zenith. The GLAO-corrected FWHM varies as a power law of air mass with an exponent of 0.875, while the power law without AO is 0.6. GLAO performance with increasing air mass will always degrade faster than in the seeing-limited case because GLAO includes fitting error. Fitting error increases at the same rate as seeing plus anisoplanatism and will therefore degrade rapidly as more layers move into the gray zone described by Tokovinin.

5.3. Laser Power Requirements

The UD Monte Carlo modeling tool was used to estimate the laser power requirements for a GLAO system. Figure 12 shows that a minimum flux of approximately 50 detected pho-

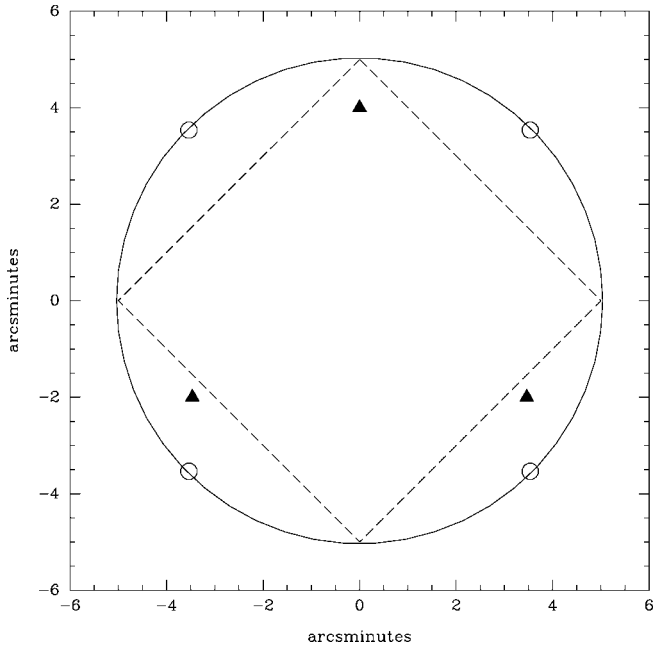

FIG. 8.—Geometry of the baseline GLAO system, consisting of four LGSs marked with open circles on a 5′ ring (*solid line*). Three NGSs are marked with filled triangles, and a 7′ × 7′ science FOV is marked with a dashed line.

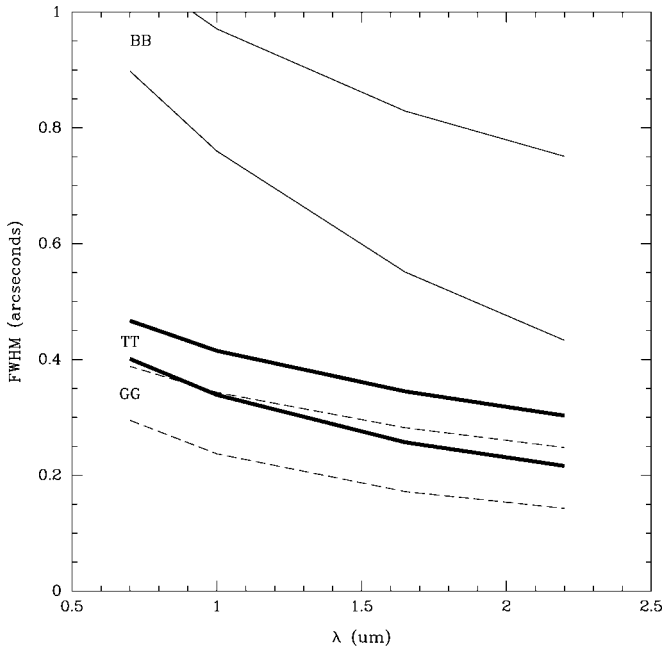

FIG. 9.—FWHM vs. wavelength λ for three model atmospheres: good : good (*dashed lines*), typical : typical (*thick solid lines*), and bad : bad (*thin solid lines*). The upper line is the seeing-limited FWHM, and the lower line is the GLAO-corrected FWHM. The correction is greatest for turbulence profiles with "bad" ground layers and at longer wavelengths. Simulations used a DM with 77 dof and a 10′ FOV.

tons per WFS subaperture per detector integration will be required to achieve close to optimal correction. We note that the model considered the LGSs to be point sources and did not include spot elongation. Treating laser beacons as point sources results in simulated WFS spots that are too small and are thus accurately centroidable with fewer photons, so the predicted AO performance at low light levels is overly optimistic. With this caveat, we found that for 227 total subapertures, a sodium laser beacon, and typical sodium layer column density, this translates to a LGS launch power less than 1 W. Although this is a lower limit on the required laser power, sufficient WFS photon flux should be achieved with a relatively low power of 2–5 W sodium LGS system. The main reasons why the required power is low compared to other laser AO systems is that the WFS signal is averaged, and the error budget for reaching the expected GLAO correction is relaxed; a GLAO system does not produce diffraction-limited images even in the near-IR, so the required laser power is minimal.

5.4. Sky Coverage

To compute the sky coverage expected for our baseline system, we used conservative estimates of the NGS noise performance drawn from our Monte Carlo simulations (Fig. 13) and assumed that (1) 100 photons per integration are required, (2) GLAO used a 500 Hz sampling rate, (3) the overall telescope plus detector efficiency was 60%, and (4) the WFS operated in the *V* band. Based on these assumptions, one needs three NGS stars with $V < 15.0$.[6] Based on the Bahcall & Soneira (1980) models of the Galaxy, there is a density of ~135 stars deg^{-2} at the Galactic pole. For each third of the 70′ × 70′ FOV, there will be an average of 0.9 stars per sector patrolled by the NGS WFS. Assuming that the number of stars are Poisson distributed and spaced randomly over the FOV, there is a 20% probability that all three NGS WFS probes can be placed on $V < 15$ guide stars and an 81% chance that at least one probe can be placed on a bright NGS while the other two probes placed on a fainter NGS read out at a slower rate (100 Hz). Only one NGS needs to be bright enough for the WFS to be read out rapidly and to control for telescope vibrations and wind shake; the gain from having three NGS WFSs versus one NGS WFS reading out at such a fast rate will be significantly less substantial.

As shown in Figure 7, the nonuniformity of PSFs across the FOV is greatest near the LGSs. NGSs have a lesser effect on the variation of PSFs (Fig. 14); the variation in PSFs introduced by NGSs is only apparent under the best atmospheric condi-

[6] The sampling rate of 500 Hz was chosen only so that GLAO could be used to remove potential telescope vibrations. If these vibrations are unimportant, a sampling rate of 100 Hz can be adopted, which leads to a limiting magnitude of $V < 16.8$ for the NGS tip-tilt stars.

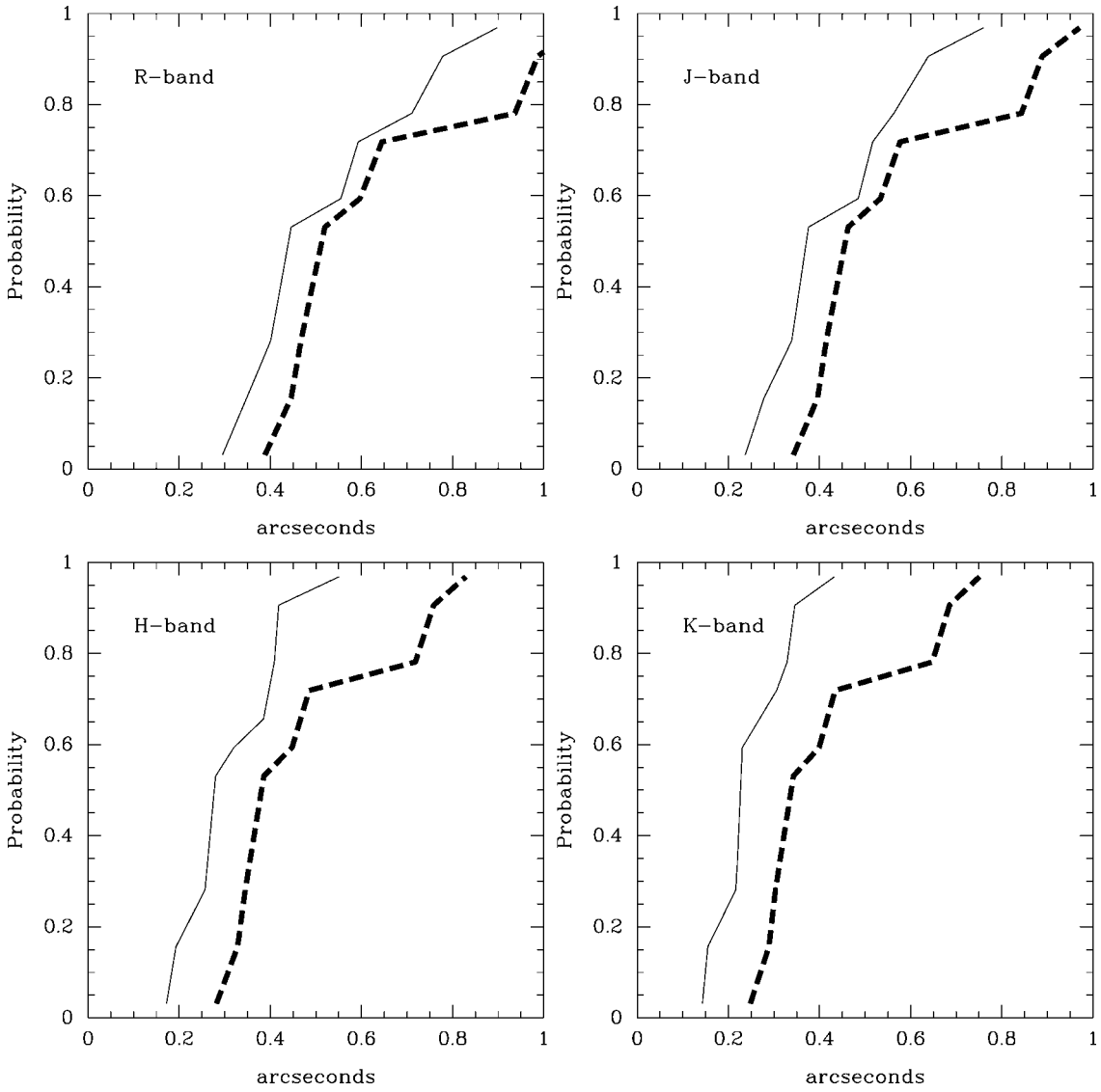

FIG. 10.—Cumulative histogram of FWHM, based on the nine model atmospheres for both seeing-limited (*dashed lines*) and GLAO (*solid lines*) cases for wavelengths of 0.70 μm (*R* band; *top left*), 1.00 μm (*J* band; *top right*), 1.65 μm (*H* band; *bottom left*), and 2.2 μm (*K* band; *bottom right*). All simulations used a DM with 77 dof and a 10′ FOV. A GLAO correction can alter the image quality statistics at a site; the relatively greater improvement when seeing is poorest (and presumably the ground-layer turbulence is greatest) means GLAO can virtually eliminate bad-seeing nights. The poorest image quality occurring 30% of the time without GLAO will only occur ~10% of the time with GLAO.

tions. In general, the PSF uniformity is still quite high over the selected FOV.

6. TRADE STUDY SIMULATIONS

Starting from this baseline model, we explore a large parameter space and track GLAO performance. We study how the performance of a GLAO system depends on the corrected field of view, the DM actuator density (or equivalently in our view, the WFS sampling), and different choices relating to the WFSs. Because we wanted to study these trade-offs over a range of relevant scientific wavelengths and the nine model atmospheres, we primarily used analytic modeling tools to carry out this work.

6.1. FOV Trade Study

Our analytic simulations show that the GLAO performance does improve as the FOV (i.e., the radius of the LGS asterism) decreases, but the dependency between FOV and performance is weak; the FWHM decreases by only 18% when the area of the FOV is increased by a factor of 6.25 (Fig. 15). This is not

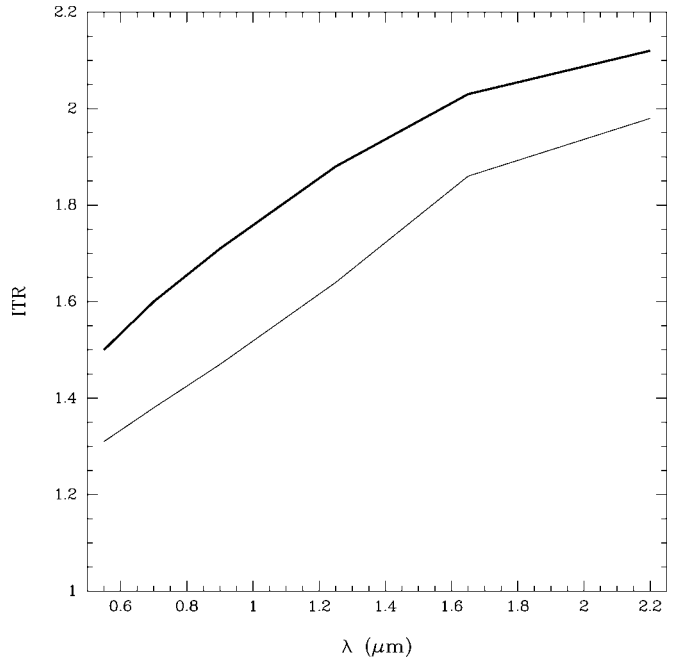

FIG. 11.—ITR as a function of wavelength, using DMs with 227 dof (*thin line*) and 2000 dof (*thick line*). This second, hypothetical DM with an enormous number of actuators represents the limit of ITR gain with a GLAO system. ITR was calculated by using a weighted sum over the nine turbulent profiles (see Table 2). Increasing the actuator density can significantly increase the performance of a GLAO system.

too surprising, as MCAO systems, which also compensate for turbulence in discreet layers, exhibit only weak dependencies on the size of the FOV (e.g., Le Louarn 2002). The factor limiting GLAO performance gains is the strength of turbulence in the free atmosphere; a simulation of the atmosphere excluding the ground layer (all layers under 1.6 km) showed that the mean seeing of a perfect GLAO system will only be 0.″28 for a wavelength of 1 μm, assuming that the simulated atmospheres and their weighted probabilities (Table 2) are reasonable, compared to the mean seeing without any adaptive optics of 0.″56.

Although the performance of a GLAO system decreases as the size of the corrected FOV increases, the overall survey efficiency (exposure time needed to survey a given area of the sky to a given limiting magnitude) increases. Since many of the primary science cases for MCAO and GLAO systems involve large surveys, we compared the relative survey efficiencies for these AO systems. The proposed Gemini GLAO imaging FOV is $49' \times 49'$, compared to $2' \times 2'$ for GSAOI (Gemini South Adaptive Optics Imager, the imager for the Gemini MCAO system). For this example, the survey efficiency of a GLAO system is 4 times that of a MCAO system for point sources. For non–point sources, the ratio of observing efficiency increases dramatically; for objects with FWHMs of 0.″3,

TABLE 5
PERFORMANCE OFF-ZENITH FOR A TYPICAL : TYPICAL ATMOSPHERE WITH A SCIENTIFIC WAVELENGTH OF 1.6 μm

	FWHM		0.″2 EE	
ZENITH ANGLE (deg)	Mean (arcsec)	rms (arcsec)	Mean (arcsec)	rms (arcsec)
0	0.299	0.013	0.211	0.006
30	0.338	0.012	0.177	0.006
45	0.401	0.012	0.137	0.004
60	0.548	0.015	0.083	0.003

GLAO has an observing efficiency 40 times that of MCAO.[7] Because this measure of survey efficiency does not include acquisition and setup times, real gains in observing efficiency are even greater when the additional overhead of setting up 25 MCAO observations to cover the same FOV as a single GLAO observation is taken into account. For planned GLAO systems, this result suggests that the GLAO FOV be made as large as possible, until the extra acquisition overhead associated with running a LGS GLAO system coupled to decreasing performance gain outweighs the increased FOV.

[7] To be fair, MCAO will yield better angular resolution for these objects, enabling more science than a mere detection.

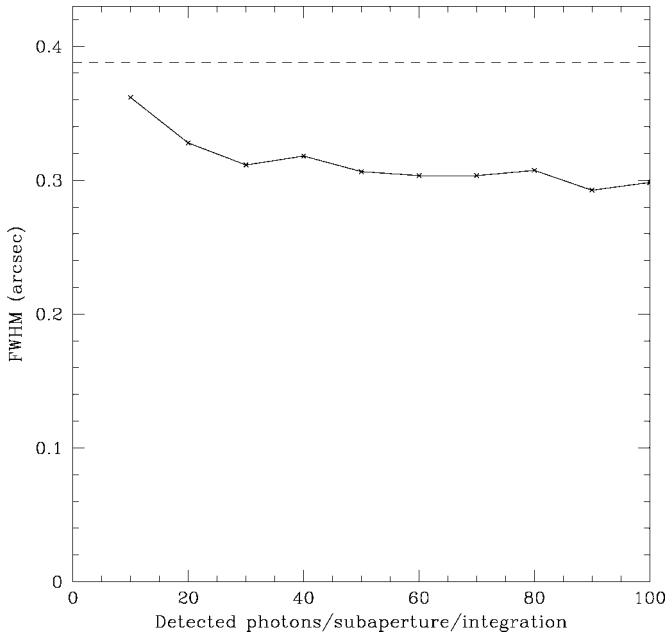

FIG. 12.—FWHM of science PSF at 1.6 μm as a function of LGS photon flux. Tip-tilt NGSs are assumed to be bright. The dashed line shows the FWHM of the uncorrected PSF. The Monte Carlo simulations assumed the LGSs were point sources. Smaller spots are easier to centroid, therefore requiring fewer photons per subaperture to be centroidable. Larger, elongated spots will require more detected photons per subaperture, making this result a lower limit on the photons required to be produced by the LGSs.

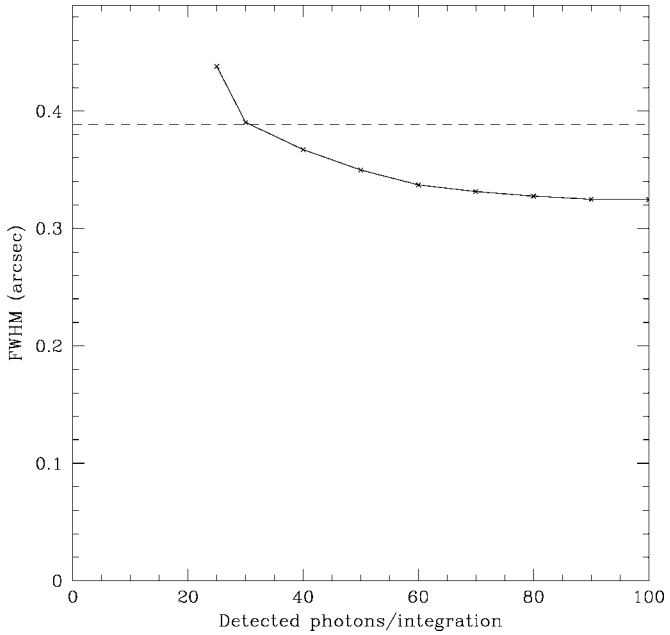

FIG. 13.—FWHM of the science PSF at 1.6 μm, as a function of NGS (tip-tilt) photon flux. LGSs are assumed to be bright. The dashed line shows the FWHM of the uncorrected PSF. A GLAO system requiring 100 photons per integration with one WFS operating at 500 Hz translates into an 81% sky coverage at the north Galactic pole (92% sky coverage is achievable with slightly diminished performance if only 60 detected photons per integration are required).

6.2. DM Property Trade Studies

6.2.1. Actuator Density

Another important dimension of the GLAO parameter space that we studied was the effect of varying actuator densities on GLAO performance. Initial simulations used a DM with 77 degrees of freedom (dof). If the actuator density of the DM were significantly increased, we postulated that the performance could improve substantially because the fitting error would decrease. We found that the optimal number of actuators depends on both the turbulence profile and the scientific wavelength. In most cases, the optimal number of actuators is actually quite large (~30 actuators across the DM, or ~700 dof). However, the performance in general is relatively insensitive to the number of actuators (Fig. 16). Only 314 dof are needed to recover 95% of the optimal GLAO performance for $\lambda > 0.7$ μm. As Figures 11 and 17 show, increasing the number of actuators has the greatest relative impact at the shortest scientific wavelength and when the free atmosphere has very little turbulence. In both of these cases, fitting error dominates over other sources of error. If the goal of a GLAO system were only to deliver improved performance in the NIR, a DM with ~80 dof would be adequate under most conditions.

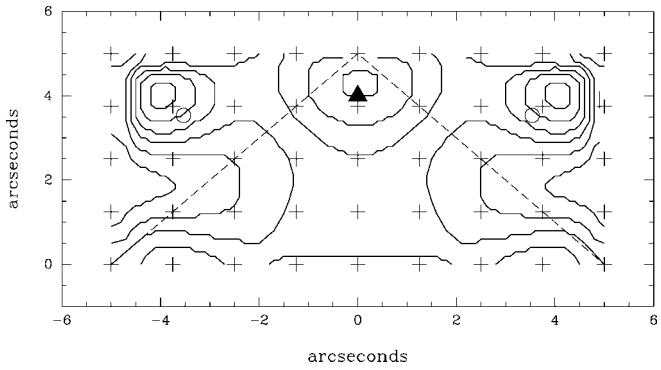

FIG. 14.—Contour plot showing a FWHM for a Monte Carlo simulation incorporating both LGS WFSs and low-order NGS WFSs, as measured at 1.65 μm for the good : good turbulence profile (which shows the strongest variations in FWHM at this wavelength). LGSs are marked by open circles, and the location of the NGS is marked with a filled triangle. Locations of simulated points are marked with plus signs. Contours are separated by 0.″05 steps in FWHM. The GLAO correction is slightly improved (by 0.″1) at the location of the NGS when compared to the field center.

6.2.2. Conjugate Altitude of DM

If the DM in a GLAO system is conjugated to an altitude that is different from the effective height of the ground-layer turbulence, one would expect anisoplanatism to degrade performance. However, analytic simulations of a DM that is not precisely conjugated to the ground-layer atmospheric altitude

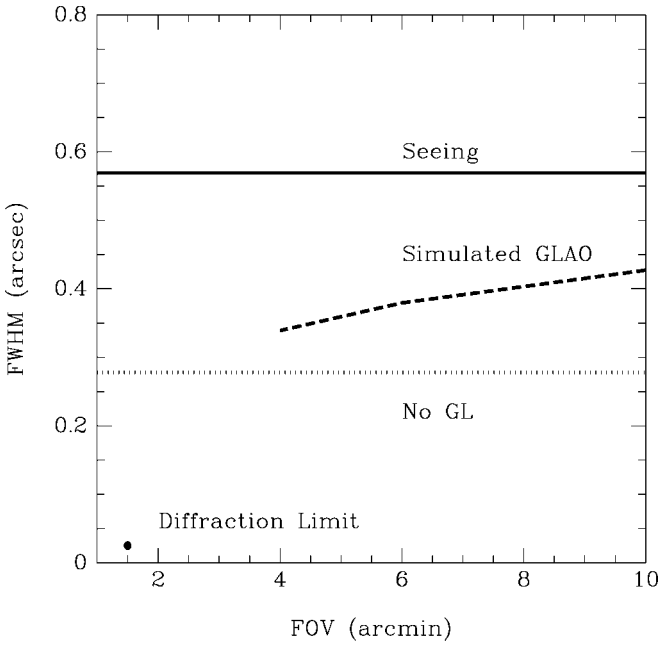

FIG. 15.—FWHM as measured at 1 μm as a function of the FOV, using the typical : typical turbulence profile. While the GLAO performance improves as field size shrinks, the gains are small; reducing the area of the FOV by a factor of 6.25 only improves the FWHM by 18%.

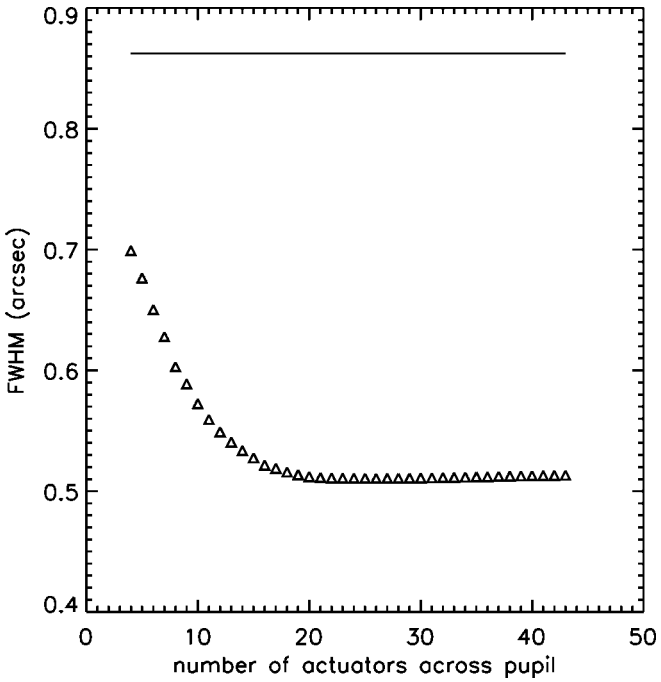

FIG. 16.—FWHM at the field center, plotted as triangles, as a function of the number of dof across the diameter of a DM. The solid horizontal line marks the seeing-limited FWHM. Simulations were performed using the bad : good profile and four LGSs at a radius of 5′ and a wavelength of 1 μm.

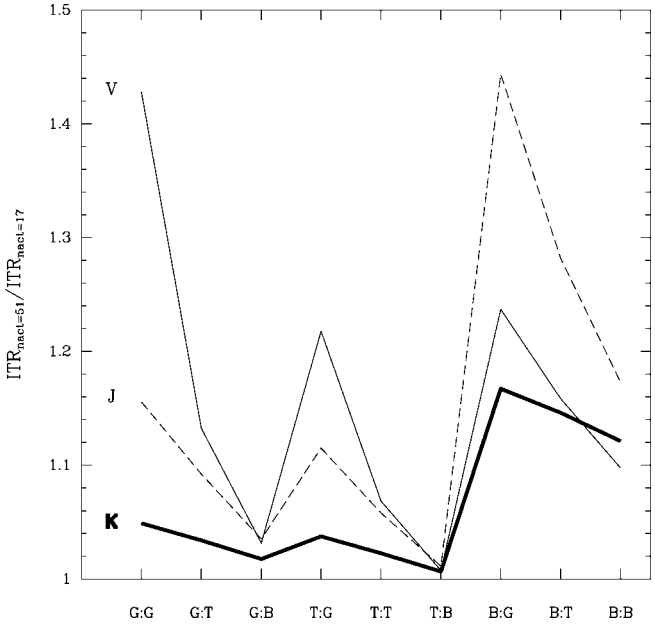

FIG. 17.—Ratio of ITR calculated using DMs with 2000 (n_{act} = 51 across diameter) vs. 227 (n_{act} = 17 across diameter) dof as a function of the different turbulent profiles (labeled ground layer : free atmosphere) for the *VJK* bands (0.55, 1.25, and 2.2 μm). The gain at the *K* band is slight because 227 actuators are sufficient to correct the ground-layer turbulence for all profiles. This is not the case in the *J* band, where it is clear that 227 actuators are not sufficient to correct all the "bad" ground-layer turbulence. Increased actuator density improves GLAO performance for "good" ground turbulence the most at shorter wavelengths. Even 2000 actuators across the DM are probably insufficient to correct the "bad" ground-layer turbulence in the *V* band, thereby limiting the gain in this regime.

show that the performance does not suffer significantly; at worst, a 5% increase in FWHM is observed for the Gemini telescopes (Fig. 18). We find that for a configuration of guide stars arranged in a pentagon, the optimal conjugation height is ~100 m, considering all results at 1–2.2 μm and all nine model profiles. Comparing the NGS pentagon to the LGS pentagon, we see that the constraint on GLAO performance from DM conjugate height misregistration is relaxed because of the cone effect. This is an important result because it means that adaptive secondary mirrors can be used with Cassegrain telescopes,[8] such as the Gemini telescopes, and still produce GLAO performance gains.

6.3. Guide Star Trade Studies

6.3.1. LGSs versus NGSs

We find that the GLAO performance is not optimal if all wave-front sensing is done using NGSs. For four real asterisms of NGSs near the north Galactic pole, the mean and standard deviation of the PSF FWHM were calculated. Variations in the PSF are 5% greater over the FOV if NGS versus LGS asterisms are used.

For one GLAO simulation using three NGSs, we looked at the morphology of the PSF in greater detail. A comparison of the FWHM for the NGS and LGS system shows again that the uniformity of the PSF FWHM is much higher for the LGS system (Fig. 19); the standard deviation in FWHM is 34 mas in this NGS GLAO simulation, compared to 8 mas for the LGS GLAO simulation. Furthermore, the correction yields an improvement in FWHM of only 0.″05, roughly half the correction achieved using the LGS system. We measured ellipticity (1 minus the axis ratio) of the isophotes corresponding to the radius of the FWHM. The magnitude and variation in ellipticity for the LGS simulation was small; the mean ellipticity is only 0.02. The change in shape of the PSF is roughly 2%. With NGSs alone, ellipticity becomes more significant: a mean ellipticity of 0.10 is observed (Fig. 19). Ellipticity is a second-order deviation; "higher order" deviations to the PSF shape appear to be negligible. Perhaps some of these disadvantages associated with using NGSs could be alleviated if even more NGSs were averaged and an optimal reconstruction algorithm were used (Nicolle et al. 2006). Of course, one other major advantage of using LGS WFSs versus NGS WFSs is that, as discussed in § 5.4, almost complete sky coverage can be

[8] The secondary mirror of a Cassegrain telescope is conjugated to below the primary mirror. For Gemini, the secondary is conjugated to 97 m below the primary.

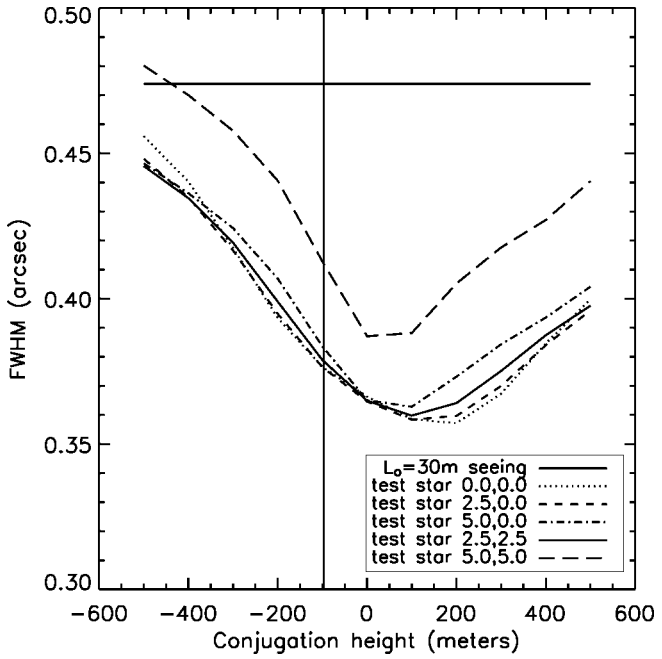

FIG. 18.—FWHM of five field positions plus the seeing-limited case (see the key), as a function of DM conjugation height. FWHMs were measured from the typical : typical profile at a wavelength of 1 μm. Considering the five field positions, the optimal conjugate altitude, depending on the image quality criteria, is around +100 m. The conjugation of the Gemini telescope secondary mirror is indicated by the vertical line at −97 m, which suffers only a 5% degradation in FWHM relative to the optimal FWHM for this case.

achieved for a GLAO system using NGS to correct only the tip-tilt.

6.3.2. Number and Geometry of LGSs

We explored GLAO performance for a range of guide star numbers and geometries. Cone effect and the altitude of the beacons were not included, which simplified the model and set aside the question of the relative placement of the high-order beacons and tip-tilt beacons that must be addressed with LGSs. Guided by the theoretical result of Tokovinin (2004) that the ideal beacon geometry for GLAO is a complete ring at the edge of the FOV, regular polygons—with and without an additional axial beacon—were explored from a triangle to a heptagon. For comparison, a single axial beacon was also investigated.

As Table 6 shows, more beacons yield slightly better results, as expected. Most of the performance gains are obtained by going from one to three LGSs. The addition of extra beacons only marginally improves the result when four or more beacons are employed. This is consistent with results reported from MCAO modeling (Fusco et al. 1999). Adding more beacons in a GLAO system means that turbulence from high layers cancels out better because more nonoverlapping high-layer turbulence volumes are measured by the WFSs. We suspect that the cancellation of high-layer turbulence in the mean wave front improves as the square root of the number of beacons.

6.3.3. Rayleigh versus Sodium Beacons

A comparison of the GLAO performance was made, in which the only difference was a change in beacon height appropriate for Rayleigh and sodium lasers. There is at best a 5% improvement if Rayleigh beacons are used, corresponding to a relatively constant ~8 mas decrease in FWHM for the model turbulence profiles. This advantage stems from the fact that the cone effect from the lower Rayleigh beacon will be greater and thus less affected by high-turbulence layers.

6.3.4. Number of Tip-Tilt Stars versus Angular Resolution

For a LGS WFS system, tip-tilt sensing is typically done with an NGS. Given the effects of anisoplanatism, a single star is inadequate to correct the full GLAO field. A minimum of three is required to provide compensation over the field in both dimensions, but the question arises as to whether even more stars would yield substantial improvements. Consequently, we investigated the level of tilt correction with two guide star geometries: both used five sodium LGSs on a circle of 10′ diameter, with either three or eight NGSs arranged as a regular polygon on the same circle. We found that three NGSs are adequate, as the magnitude of the FWHM improvement by using eight NGSs was only 10% greater than when three NGSs were used (i.e., for a ~0.″1 decrease in the GLAO FWHM, increasing the number of NGSs essentially decreased the FWHM by just ~0.″01).

7. SUMMARY

We have used the best available measures of ground-layer turbulence profiles and a suite of modeling tools to study the performance of a GLAO system. This work is the most complete study of GLAO to date, and our results serve to "demystify" GLAO. Among the many results of this study, we highlight the following:

1. The shape of the GLAO PSF is qualitatively the same as a seeing-limited PSF. Therefore, while having complete knowledge of the PSF is desirable, the FWHM of the PSF is a practical and useful general metric for measuring GLAO performance. Other performance metrics are more appropriate for specific applications; e.g., integration time ratio is ideal for background-limited imaging, and ensquared energy is the most useful metric for spectroscopic observations.

2. A GLAO system would significantly improve the image quality statistics. Unlike traditional AO systems, some of the greatest gains to be had with GLAO are obtained when the seeing is poor. In effect, this means that the number of nights

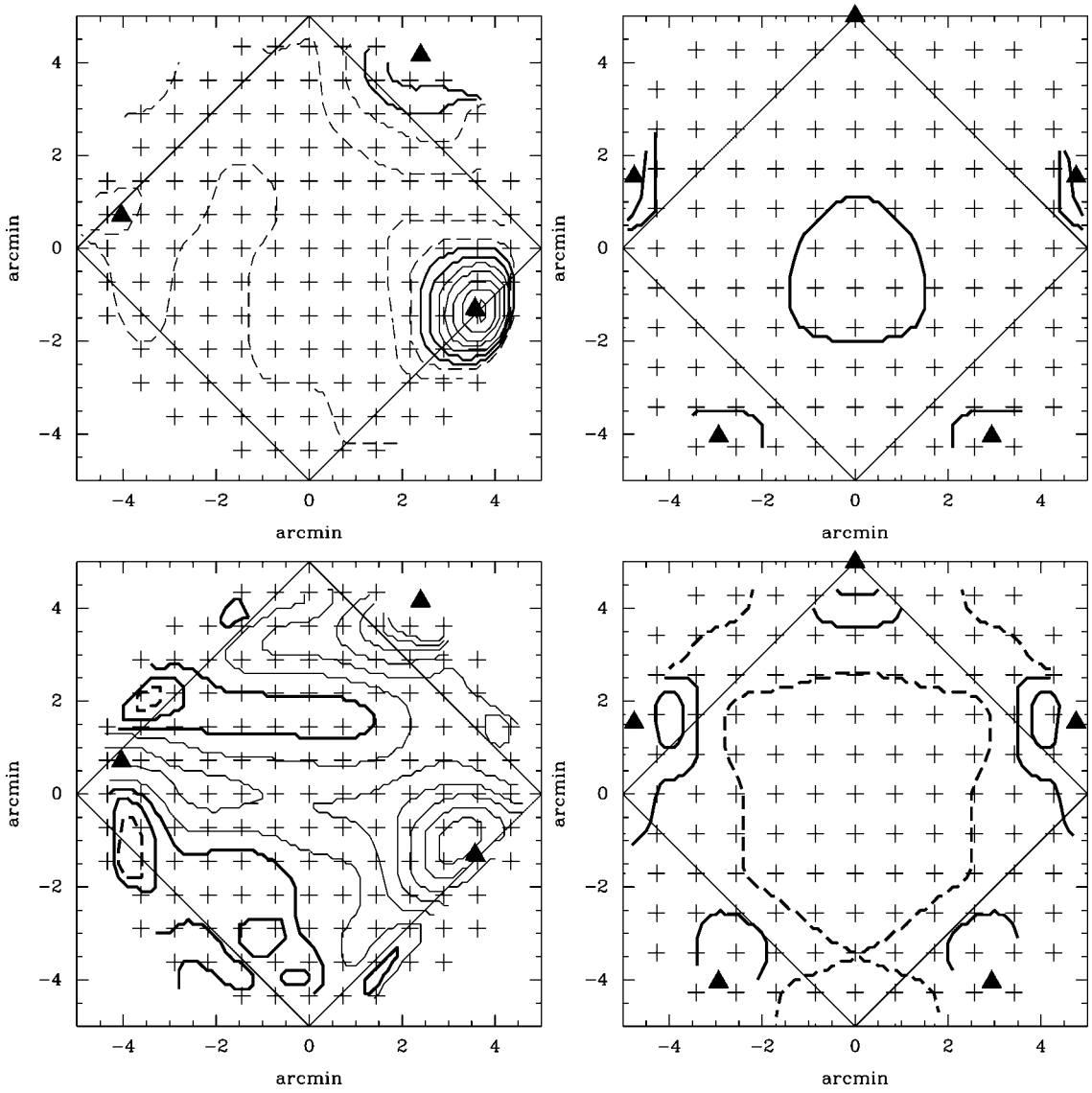

FIG. 19.—Comparison of GLAO correction using three NGSs of different brightnesses scattered randomly over the field (*left panels*) or five LGSs arranged in a regular pentagon (*right panels*). For each guide star asterism (*filled triangles*), we show contours of FWHM (*top panels*) and ellipticity (*bottom panels*). The FWHM is smaller when LGSs are used (top panels have the same contours marked with thick lines); the contours, separated by 0″.02, show that the NGS correction is between 0″.02 and 0″.04 worse over the majority of the FOV. More importantly, for PSF calibration, the shape of the PSF is uniform when a regular asterism is used. In the ellipticity figures, the lowest measured ellipticity contour ($1 - b/a = 0.02$ of the PSF measured at the FWHM) is marked with a dashed line and is a good description for most of the FOV when LGSs are used. The ellipticity in the PSF is as high as 0.14 within the FOV for the NGS case (contours are separated by 0.02 in ellipticity). Locations of the simulated PSFs are marked by plus signs, and a $7' \times 7'$ FOV is marked on each figure as well.

with image quality worse than the current 70% level should be drastically reduced.

3. Because diffraction-limited imaging is not the goal of GLAO, almost complete sky coverage is obtainable, and the corresponding laser power requirements for a GLAO system are low.

4. The performance of a GLAO system is relatively insensitive to a large number of trade-offs. The performance is not a strong function of the corrected FOV, the actuator density of the DM, the conjugate height of the DM, the height of the LGS, or the guide star geometry.

5. While our GLAO modeling of very wide fields showed that performance gains are not as large as previously reported, the substantial gains we do find would translate into major

TABLE 6
FIELD-AVERAGED FWHM FOR EACH GUIDE STAR GEOMETRY, USING THE GOOD : GOOD, TYPICAL : TYPICAL, AND BAD : BAD CERRO PACHÓN TURBULENCE PROFILES

Guide Star Geometry	Good : Good	Typical : Typical	Bad : Bad
1	0.293 ± 0.027	0.471 ± 0.043	0.845 ± 0.070
3	0.230 ± 0.007	0.382 ± 0.012	0.727 ± 0.017
3+1	0.217 ± 0.008	0.361 ± 0.014	0.696 ± 0.025
4	0.221 ± 0.006	0.368 ± 0.009	0.708 ± 0.014
4+1	0.212 ± 0.007	0.354 ± 0.011	0.687 ± 0.021
5	0.215 ± 0.006	0.359 ± 0.009	0.694 ± 0.013
5+1	0.209 ± 0.006	0.348 ± 0.010	0.678 ± 0.018
6	0.212 ± 0.003	0.354 ± 0.004	0.688 ± 0.007
6+1	0.207 ± 0.004	0.346 ± 0.007	0.674 ± 0.015
No GLAO	0.351	0.474	0.992

NOTES.—Measurements were made for a scientific wavelength of 1 μm and a 10′ diameter FOV. Guide stars are evenly spaced around this diameter, unless the configuration is denoted (e.g., 3+1), in which case one LGS is located at the center of the FOV.

increases in the number of scientific programs that can be completed within a given time on large telescopes. Installing a GLAO system on a large telescope would increase the observing efficiency by at most 40%.

6. GLAO is highly complementary to other modes of AO. GLAO can improve image quality in the optical and under intrinsically poor image quality conditions in which more traditional AO systems are unusable, especially if a system with several hundred dof is implemented. GLAO also yields the greatest survey efficiency; as we have shown, the survey efficiency of a GLAO system continues to increase with the FOV and should be much greater than the MCAO survey efficiency. MCAO and classical AO could be used with a GLAO survey instrument for follow-up observations of the most exciting targets. In addition, the sky coverage of a GLAO system will be greater than that of traditional AO systems, due to the increased FOV and the insensitivity of the performance to most of the studied variables.

The authors wish to thank S. Shectman for his useful comments, and Gemini Observatory and its staff for their contributions.

REFERENCES

Babcock, H. W. 1953, PASP, 65, 229
Bahcall, J. N., & Soneira, R. M. 1980, ApJS, 44, 73
Baranec, C. J., Lloyd-Hart, M., Codona, J. L., & Milton, N. M. 2003, Proc. SPIE, 5169, 341
Beckers, J. M. 1989, The NOAO 8 m Telescope Technical Description, Vol. 2 (Tucson: NOAO)
———. 2000, Proc. SPIE, 4007, 1056
Dekany, R., Bouchez, A., Britton, M., Velur, V., Mitchell, T., Shelton, J. C., & Roberts, J. 2006, Proc. SPIE, 6272, 627209
Ellerbroek, B. L. 2005, J. Opt. Soc. Am. A, 22, 310
Flicker, R., Rigaut, F. J., & Ellerbroek, B. L. 2000, Proc. SPIE, 4007, 1032
Foy, R., & Labeyrie, A. 1985, A&A, 152, L29
Fusco, T., Conan, J.-M., Michau, V., Mugnier, L. M., & Rousset, G. 1999, Opt. Lett., 24, 1472
Hubin, N. N., et al. 2004, Proc. SPIE, 5490, 846
Johnston, D. C., & Welsh, B. M. 1991, Proc. SPIE, 1542, 76
Jolissaint, L., & Véran, J.-P. 2002, in Beyond Conventional Adaptive Optics, ed. E. Vernet et al. (Garching: ESO), 201
Jolissaint, L., Véran, J.-P., & Conan, R. 2006, J. Opt. Soc. Am. A, 23, 382
Jolissaint, L., Véran, J. P., & Stoesz, J. A. 2004, Proc. SPIE, 5382, 468
Le Louarn, M. 2002, MNRAS, 334, 865
Le Louarn, M., & Hubin, N. 2004, MNRAS, 349, 1009
Lloyd-Hart, M., & Milton, N. M. 2003, Proc. SPIE, 4840, 18
Moffat, A. F. J. 1969, A&A, 3, 455
Nicolle, M., Fusco, T., Michau, V., Rousset, G., & Beuzit, J.-L. 2006, J. Opt. Soc. Am. A, 23, 2333
Ragazzoni, R. 1999, in ESO/OSA Topical Meeting on Astronomy with Adaptive Optics, ed. D. Bonaccini (Garching: ESO), 651
Ragazzoni, R., Farinato, J., & Marchetti, E. 2000, Proc. SPIE, 4007, 1076
Rigaut, F. 2002, in Beyond Conventional Adaptive Optics, ed. E. Vernet et al. (Garching: ESO), 11
Stoesz, J. A., Jolissaint, L., Véran, J.-P., & LeDue, J. 2004, Proc. SPIE, 5490, 713
Tokovinin, A. A. 2002, in Beyond Conventional Adaptive Optics, ed. E. Vernet et al. (Garching: ESO), 183
———. 2003, MNRAS, 340, 52
———. 2004, PASP, 116, 941
Tokovinin, A., Baumont, S., & Vasquez, J. 2003, MNRAS, 340, 52
Tokovinin, A., & Travouillon, T. 2006, MNRAS, 365, 1235
Tokovinin, A., & Viard, E. 2001, J. Opt. Soc. Am. A, 18, 873
Vernin, J., et al. 2000, Gemini RPT-AO-G0094 (Hilo: Gemini Obs.), http://www.gemini.edu/documentation/webdocs/rpt/rpt-ao-g0094-1.ps